PCCP

Selective Photo-Excitation of Molecules Enabled by Stimulated Raman Pre-Excitation

Journal:	*Physical Chemistry Chemical Physics*
Manuscript ID	CP-ART-02-2022-000868.R1
Article Type:	Paper
Date Submitted by the Author:	30-Mar-2022
Complete List of Authors:	Wang, Yisen; Chinese Academy of Sciences Guangzhou Branch, GBA Branch of Aerospace Information Research Institute Laforge, Francois; Princeton University, Chemistry Goun, Alexei; Princeton University, Department of Chemistry Rabitz, Herschel; Princeton University, Department of Chemistry

PCCP

ARTICLE TYPE

Cite this: DOI: 00.0000/xxxxxxxxxx

Selective Photo-Excitation of Molecules Enabled by Stimulated Raman Pre-Excitation†

Yisen Wang,[a] Francois Laforge,[b] Alexei Goun[b] and Herschel Rabitz*[b]

Received Date
Accepted Date

DOI: 00.0000/xxxxxxxxxx

Double resonance excitation, where the energies of vibrational and electronic molecular transitions are combined in a single, sequential excitation process, was introduced in the 1970s but has only been recently applied to microscopy due to the immense progress in Raman spectroscopy. The value of the technique is in combining the chemical selectivity of IR or Raman excitation with the much larger cross-sections of electronic transitions. Recently, it has been shown to be particularly suited for the detection and identification of chromophores at low concentrations and in the presence of spectral crosstalk. However, despite its low quantum yield per pulse sequence, we believe the technique has potential for selective photochemical transformations. There are some cases (e.g., the selective excitation of optogenetic switches) where the low yield may be overcome by repeated excitations to build up biochemically relevant concentrations. Here we show that double resonance excitation using general, non-resonant Raman pre-excitation is a viable candidate for selectively promoting molecules to chemically active energy levels. The use of non-resonant Raman pre-excitation is less constraining than resonant Raman (used in previous double resonance microscopy works) since the choice of Raman pump-Stokes frequencies may be rather freely chosen.

1 Introduction

Double resonance excitation schemes, where vibrational and electronic transitions are combined in a single, sequential excitation process, were first explored in the late 1970s using IR pulses to pump vibrational modes[1,2]. However the technique was unsuccessful when pre-exciting with a stimulated Raman process due to other strongly competing non-linear effects[3,4]. Progress done in ultrafast laser technology, stimulated Raman scattering (SRS) spectroscopy[5–8] and fluorescence microscopy[9–11] over the past two decades has made the double resonance technique applicable to microscopy, especially when detecting and identifying low concentrations of chromophores in the presence of spectral crosstalk. Fig. 1 shows the principle of selective double resonance excitation with SRS as pre-excitation. (a) and (b) are the energy diagrams of two molecules that have similar electronic absorption spectra but different vibrational spectra. In case (a) the pump-Stokes pulse pair is out of resonance with the Raman transition as is the actinic excitation beam with respect to the electronic transition. Molecule (a) therefore cannot be excited to its first electronic excited state. In case (b) the pump-Stokes pair is resonant with a Raman transition and populates a ground state vibronic level thus the actinic beam can transfer the latter population to the first electronic excited state.

Xiong et al recently applied the method discussed in Fig. 1(b) to develop an imaging technique with exquisite chemical selectivity and superb sensitivity that they named *stimulated Raman excited fluorescence* (SREF)[12,13]. To increase the SRS cross section by up to five orders of magnitude they operated in the resonant SRS regime where the central wavelength of the pump pulse lies in the electronic pre-resonance region of the target chromophore.

Double resonance excitation may also be used to photoactivate chemical processes. Despite its low yield (compared to direct electronic excitation), its selectivity would be advantageous when operating in a mixture of spectrally overlapping reactants. Moreover, for the sake of generality, using non-resonant SRS as the pre-exitation step would not only free users from constraints on the pump, Stokes and probe frequencies (other than achieving double resonance), but also permit independently optimizing the frequencies and shapes of the three pulses.

Here we demonstrate double resonance excitation using a non-resonant SRS pulse pair and a femtosecond actinic pulse. To allow for the possibility of exciting non-fluorescing molecules, we detect double resonance excitation by observing the change in absorption of the target molecule.

[a] *GBA Branch of Aerospace Information Research Institute, Chinese Academy of Sciences, Guangzhou 510535, China.*
[b] *Department of Chemistry, Princeton University, Princeton, New Jersey 08544, USA. Tel: 609-258-3917; E-mail: hrabitz@princeton.edu*
† Electronic Supplementary Information (ESI) available: Additional experimental details, materials, and methods. See DOI: 10.1039/cXCP00000x/

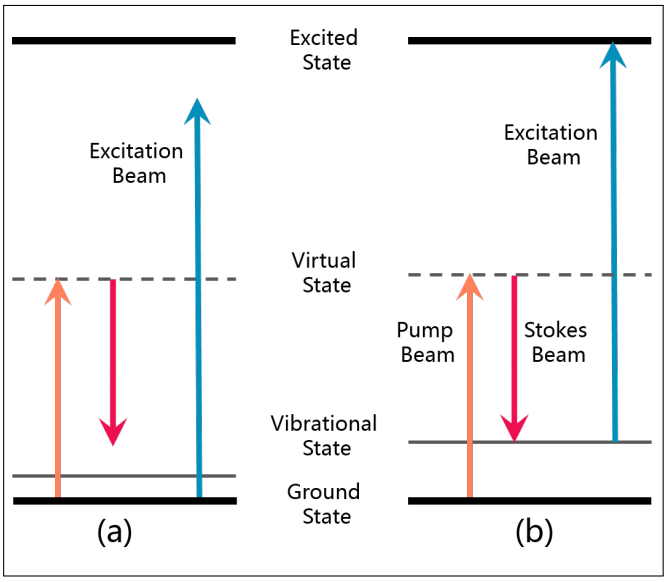

Fig. 1 The double resonance excitation method with SRS as the pre-excitation step. Molecules (a) and (b) have overlapping direct electronic absorption spectra. The pump-Stokes pulse pair match a Raman transition in (b) but not in (a); subsequent selective excitation occurs in (b).

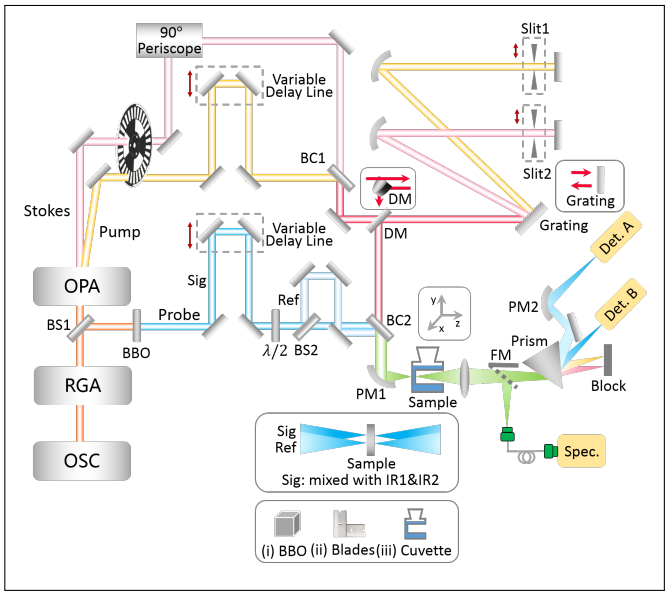

Fig. 2 Schematic illustration of the experimental setup. BS, beam splitter; BC, beam combiner; DM, D-shape mirror; PM, parabolic mirror; FM, foldable mirror. To precisely align the three beams, (i) BBO, (ii) Razor blades and (iii) Cuvette are put at the PM focus, in sequence. The BBO is for coarse alignment of spatial overlap and fine temporal overlap, razor blades are used to fine tune spatial overlap just before putting in the sample cuvette. See supplementary material section Sec. 2 for further details about the alignment procedure.

2 Experimental Results

2.1 Selective excitation detection scheme

Fig. 2(a) shows the experimental setup. The output of a regenerative amplifier (810 nm, 40 fs, 1.8 W average power, 1 kHz repetition rate) is split in two arms. One arm is doubled with a BBO crystal to produce a probe beam (λ_{Probe} = 405 nm), the other arm is input to an OPA which delivers a pump beam with central wavelength λ_{Pump} = 1460 nm and a Stokes beam with central wavelength λ_{Stokes} = 1838 nm. The pump and Stokes pulses' duration were not measured experimentally but are specified to be within 40 to 130 fs by the OPA manufacturer. The pump-Stokes pair can be further spectrally filtered with a 4f pulse shaper setup. Two delay lines permit delaying the Stokes and probe pulses independently with respect to the pump pulse. All beams are linearly polarized; both pump and Stokes beams are vertically polarized while the polarization of the probe beam can be continuously rotated with a half-wave plate. The three beams are made collinear and focused in the sample with a 45° gold-plated parabolic mirror (f=25.4 mm). Further details about the experimental setup can be found in Sec. 1 of the supplementary material. Because of the large spread in wavelengths (∼1800 nm to ∼400 nm) only a parabolic mirror can ensure achromaticity and focus the three beams at the same distance. Precise spatial and temporal overlap of the three beams was achieved using an alignment procedure that is described in Sec. 2 of the supplementary material. To maximize the generation of the Raman induced change in absorption (see below) while minimizing other undesirable effects, we use a sample cell whose 100 μm thickness matches the Raleigh length of the focused beams. The sample consists of a solution of 1-chloroanthracene in benzene with a concentration of 0.75 M to achieve a transmission of ∼10% at 405 nm. No 1-chloroanthracene aggregation was observed since a plot of absorbance vs 1-chloroanthracene concentration remained linear up to 1.17 M (see Fig. S3 in Sec. 5 of the supplementary material). Neither the pump nor the Stokes beam was significantly absorbed by the solution.

The purpose of the experiment is to measure an increase in absorbance δA ($A = -log_{10}[I/I_0]$) due to a transient change of concentration of vibrationally excited molecules. The absorbance is related to the concentration via the molar extinction by the Beer-Lambert law $A(\lambda) = \varepsilon(\lambda)cl$ where λ is the wavelength, c the total concentration of the absorbing molecule and l the path length of the sample cell. At the probe wavelength (i.e., ∼405 nm) the absorption is mainly due to that portion of 1-chloroanthracene molecules which are vibrationally excited, the so-called hot band absorption (see Sec. 2.2 below). Signal noise may arise from (1) shot-to-shot variations of the probe pulse's fluence, (2) fluctuations of δA (themselves mainly due to shot-to-shot variations of the IR pulses' fluence and beam pointing fluctuations) and (3) recording electronics. The electronics recording noise is negligible compared to the two other noise sources. To reduce the noise caused by shot-to-shot variations of the probe pulse's fluence during signal averaging, we split the probe beam into a reference beam and a signal beam before the sample. The reference beam is not collinear to the other beams but goes through the same optics (including the sample) while focusing slightly away from the other beams. We use two identical home-made silicon photodetectors to simultaneously record the fluence of the reference and signal pulses after passing through the sample for each shot. Each detector gain can be independently adjusted. Although the sensitivity of the silicon photodetectors is extremely small at the

IR wavelengths used, some signal from the IR beams could be observed. We dispersed the beams after the sample to filter out the IR so that only the signal and reference beams would be recorded. At the reference detectors, the signal can be written as

$$F_{ref} = rg_{ref}F_0 \int G(\omega)10^{-\varepsilon(\omega)cl}d\omega \quad (1)$$

while at the signal detector, it can be written as

$$F_{sig} = (1-r)g_{sig}F_0 \int G(\omega)10^{-\varepsilon(\omega)[c+\delta c]l}d\omega. \quad (2)$$

F_0 is the probe pulse's fluence before the beam splitter and $G(\omega)$ is the product of the spectral quantum yield of the silicon photodetectors and the normalized spectral intensity of the probe pulse. $\varepsilon(\omega)$ is the extinction coefficient, c (δc) is the total (excess vibrationally excited) concentration of absorbing molecules and l the path length of the sample cell. r is the beam splitter ratio, g_{ref} and g_{sig} are the gains of the reference and signal detectors, respectively. The integration is over the ~7 nm bandwidth of the probe pulse.

Dividing Eq. 2 by Eq. 1 we can express the normalized signal $S = F_{sig}/F_{ref}$, and for small changes in the concentration of vibrationally excited molecules:

$$S \approx k(1-h\delta c/c) \quad (3)$$

where $k = (1-r)g_{sig}/rg_{ref}$ and

$$h = \ln 10 lc \int G(\omega)\varepsilon(\omega)10^{-\varepsilon(\omega)lc}d\omega \Big/ \int G(\omega)10^{-\varepsilon(\omega)lc}d\omega.$$

Because F_0 doesn't appear in Eq. 3, S is independent of the shot-to-shot noise in the probe pulse fluence (for an example of the shot-to-shot noise cancellation see Fig. S1 in supplementary material Sec. 3). The constant k can be made unity by adjusting the gains of the reference or signal detectors. h represents the averaged absorbance of the solution over the probe bandwidth multiplied by the the quantum efficiency of the detectors.

To deal with the noise originating from fluctuations in the fluence of the Raman pulse pair we used a double frequency chopping scheme[14]. The pump and Stokes pulses are chopped at 500 Hz and 50Hz, respectively, with a dual frequency chopper blade. The pulse sequence repeats every 20 probe pulses (i.e., every 20 ms). A time sequence of the pulses and trigger signals is shown in Fig. S2 of supplementary material Sec. 4. In the pulse sequence there are five probe pulses when both pump and Stokes pulses are blocked, these signals can be summed up to give the background signal, S_{bkgnd}. There are also five probe pulses when the pump pulses are blocked, these signals can be summed up to give $S_{Stokes} + S_{bkgnd}$. When the Stokes pulses are blocked the signal is $S_{pump} + S_{bkgnd}$, while when all beams are allowed to pass through the sample, the signal is $S_{pump,Stokes} + S_{Stokes} + S_{pump} + S_{bkgnd}$. Thus, adding the signals when both pump and Stokes pulses are either blocked or allowed, and subtracting the signals when only pump or Stokes pulse is blocked filters out $S_{pump,Stokes}$. The extracted signal is proportional to the relative change in concentration due to the combined action of the pump-Stokes pulse pair,

$$S_{pump,Stokes} \propto -h\delta c/c. \quad (4)$$

The theory of molecular vibrational excitation through stimulated Raman scattering is well established[15]. The Raman effect is a consequence of the change in the molecular polarization tensor α with respect to the normal mode displacement $q(t)$. When the change is isotropic all the components vanish except for $(\frac{\partial\alpha}{\partial q})_{xx}$, $(\frac{\partial\alpha}{\partial q})_{yy}$ and $(\frac{\partial\alpha}{\partial q})_{zz}$ which are then all equal to a. Assuming that the pump and Stokes beams are not significantly depleted when passing through the 100 μm thick sample, all quantities are independent of the propagation direction and the fundamental equations of the Raman effect are simplified. The macroscopic vibrational polarization Q as well as the excess vibrational population n are given by[15] (see Appendix)

$$Q(t) = \kappa_2 \int_{-\infty}^{t} E_P(\tau)E_S^*(\tau)\exp(\frac{\tau-t}{T_2})d\tau \quad (5)$$

$$n(t) = \frac{aN}{8\hbar}\int_{-\infty}^{t}[E_P(\tau)E_S^*(\tau)Q^*(\tau) + E_P^*(\tau)E_S(\tau)Q(\tau)] \times \exp(\frac{\tau-t}{T_1})d\tau. \quad (6)$$

with E_P and E_S being the slowly-varying complex envelopes of the pump and Stokes E-fields, respectively.

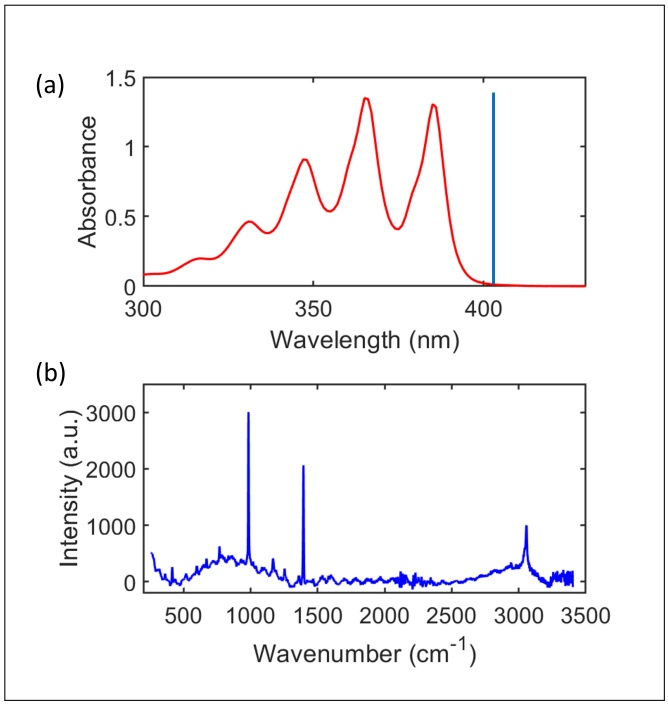

Fig. 3 (a) Absorption spectrum of 1-chloroanthracene in benzene. The blue vertical line is located at the probe beam's wavelength. (b) Raman spectrum of 1-chloroanthracene in benzene, the first main peak at ~933 cm^{-1} is the feature of benzene, the second main peak at 1403 cm^{-1} is the feature of 1-chloroanthracene.

2.2 Illustrative example

Fig. 3(a) shows the absorption spectrum of a 2 mM solution of 1-chloroanthracene in benzene taken with a 1 mm path quartz cuvette. The spectrum displays a regular progression of peaks starting at 385 nm down to 317 nm. 1-chloroanthracene spectrum is very close to that of anthracene in mildly polar solvents[16,17] except for being red-shifted by ∼10 nm. We note that the spectra of 1-chloroanthracene in benzene (Fig. 3(a)) and anthracene in ethanol(see reference[16]) have similar interpeak spacing of ∼1410 cm^{-1}. Anthracene's spectrum includes a 0←1 hot band in its tail at 400 nm. Although the band peak is about ∼1000 times smaller than the absorption maximum, the actual 0←1 transition probability is slightly higher than the 0←0 transition[17]. We expect 1-chloroanthracene to possess a 0←1 hot band with similar characteristics with a shifted maximum at 410 nm, since the 1-chloro substitution only slightly affects the molecule's spectral properties. Thus, the 405 nm central wavelength of the probe beam should fall into 1-chloroanthracene's hot band.

Fig. 3(b) shows the Raman spectrum of 1-chloroanthracene in benzene. The peak around 997 cm^{-1} is from benzene, and the peak around 1403 cm^{-1} is from the ν_6 ring deformation mode of 1-chloroanthracene[18]. Our setup can generate Raman pump-Stokes pulse pairs with energy differences varying from 1247 cm^{-1} to 1602 cm^{-1} encompassing 1-chloroanthracene's Raman peak.

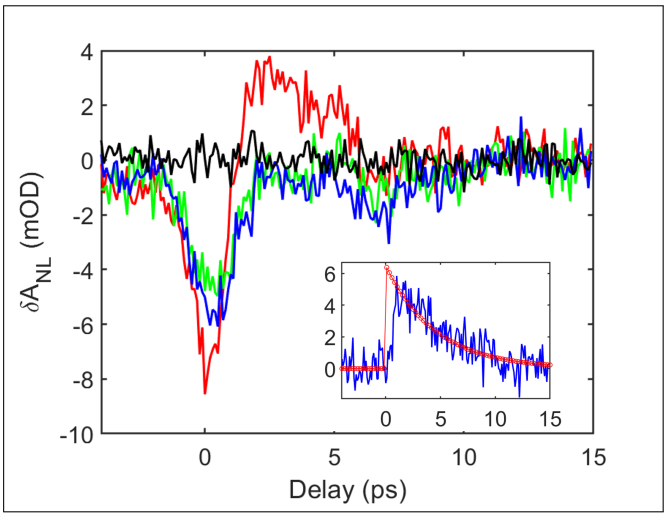

Fig. 4 Change of absorption as a function of probe delay. Red curve: the pump-Stokes pulse pair is temporally overlapped. Green (blue) curve: a delay of 3 ps (-3 ps) is introduced between the pump and the Stokes beam. Black curve: same as red curve but with neat benzene. Inset: see text for details.

In a first set of measurements, we kept the pump and Stokes beams temporally overlapped and set their central wavelengths at 1460 nm and 1838 nm, respectively to excite 1-chloroanthracene ν_6 Raman band. The 2 mm slit apertures in the 4f shaper narrows both pulses bandwidths to ∼47 cm^{-1} and consequently stretch their duration to ∼ 310 fs. Then we scanned the probe delay with a motorized translation stage from -4 ps to 15 ps. To further improve the signal-to-noise ratio (SNR) we averaged 1000 pulse sequences for every data point on the figure. The red trace in Fig. 4 shows the change in absorbance. We can see that at negative times (i.e., before the arrival of the pump-Stoke pulse pair) there is no change in absorption but after t=∼2 ps the presence of vibrationally excited molecules (above the concentration at thermal equilibrium) increases absorption. To verify that our signal arose from the expected populating of vibrationally excited 1-chloroanthracene molecules, we conducted a series of checks. The black curve is a repeat of the above experiment in neat benzene. The curve is flat since benzene is transparent at 405 nm and has a mismatched Raman peak at 997 cm^{-1}. The green and blue curves are the absorption change when the pump pulse is delayed by either +3 ps or -3 ps with respect to the Stokes pulse (longer delays give the same results). It is clear that there is no special

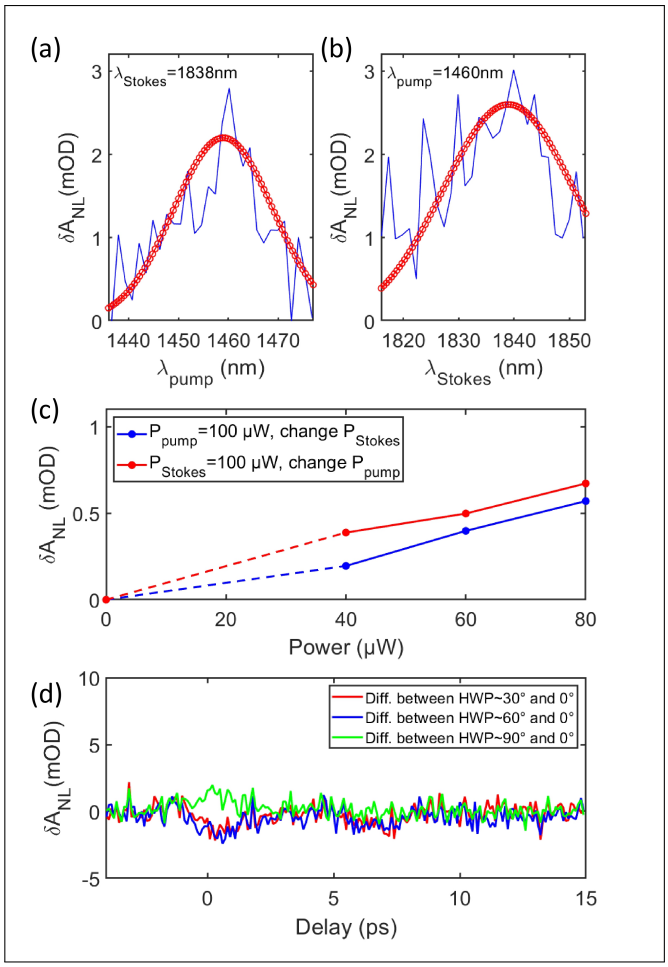

Fig. 5 (a) Pump wavelength dependence of the induced absorption 2.6 ps after pump-Stokes pre-excitation with λ_{Stokes} fixed at 1838 nm. (b) same as (a) but with Stokes wavelength varying and λ_{pump} fixed at 1460 nm. (c) Power dependence of the induced absorption on individual pump or Stokes pulses' fluence. (d) Difference of the signals when rotating the half wave plate relative to the signal when the half wave plate is at 0° .

effect from the arrival of the pump pulse since the two curves are similar. However, a negative change in absorption (i.e., generation of ∼405 nm photons) is observed when the Stokes and probe beams overlap in time probably due to four wave mixing. A smaller dip is observed at ∼7 ps whose origin is unclear. By

subtracting the average of the blue and green curves from the red curve, we obtain the change of absorption due to the Raman pumping only which is displayed in the inset of Fig. 4. The absorption increases during the action of the pump-Stokes pulse pair then decreases exponentially. A fit to an exponential, gives the rate of decay of the excess vibrational excitation of 4.5 ps. This is to be compared to a much longer value of 25 ps in the case of anthracene dissolved in C_2Cl_4 [17]. In our case, the surrounding benzene molecules might provide better vibrational coupling thus enhancing the energy transfer to the solvent leading to a faster temperature equalization.

Raman pre-excitation is key to the selectivity of the method. In a second set of experiments we measured the dependence of the change of absorption on the Pump or Stokes pulses central wavelengths. A fixed delay of 2.6 ps between the probe pulse and the pump-Stokes pulse pair was chosen to observe maximum Raman-induced changes in absorption. The 4f shaper permits tuning λ_{pump} and λ_{Stokes} from 1435 nm to 1480 nm and from 1815 nm to 1855 nm, respectively. The slit aperture was around 2 mm for both pulses to narrow their bandwidths. Because the spectral power of both filtered beams varied slightly over their respective tuning ranges (data not shown) the curves in Fig. 5(a) and (b) were normalized by the power spectrum of the tuned beam. Fig. 5(a) show the change in absorption while scanning λ_{pump} and setting λ_{Stokes}=1838 nm. The red curve is a Gaussian fit of the data with a peak at λ_{pump}=1460 nm and a FWHM of $\sim$33 nm. A similar set of data was obtained by scanning λ_{Stokes} and setting λ_{pump}=1460 nm (see Fig. 5(b)). A Gaussian fit gives a maximum at λ_{Stokes}=1838 nm and a FWHM of $\sim$27 nm. The difference of energy between the two peaks is around 1409 cm^{-1} which is close to 1-chloroanthracene main Raman line.

Another important feature of the double resonance excitation is that the observed signal should linearly depend on the power of the Pump as well as that of the Stokes beam. This can be seen from Eqs. 10 (see Appendix) as n(x,t) depends on the square of both the pump and Stokes E-field amplitudes. Fig. 5(c) shows the dependence of the signal while independently varying the pump and Stokes beam power. A close to linear trend is observed for both.

Finally, in the derivation of Eqs. 5 and 6 the assumption was made that the Raman polarizability of 1-chloroanthracene is isotropic. In that case 1-chloroanthracene molecules should be pre-excited independently of their orientation in solution. This can be verified by measuring the change in absorption as the probe polarization is changed vs that of the pump-Stokes pair. We inserted a half wave plate in the arm of the probe beam and measured the change of absorption vs the probe delay (i.e., same as red curve in Fig. 4), then we rotated the half wave plate to different positions around 30°, 60° and 90°. Fig. 5(d) shows the signal relative to the initial half wave plate position. From the figure we can see that the signal is independent of the polarization of the probe beam (except at time t=0 when four wave mixing occurs).

3 Conclusion

In summary, we have shown that double resonance excitation enabled by Raman pre-excitation is successful even when the pump-Stokes pulses' frequencies are far from any electronic resonance of the targeted molecule. A strong advantage in using non-resonant Raman pre-excitation is that the frequencies of the Raman pump and actinic pulses need not be close thus, a broader choice of target molecules and Raman pre-exciation frequencies is afforded.

Although the overall quantum yield per shot is low, the technique could be used to effect selective photo-induced chemical change. For example, bidirectional optogenetic switches, which are two-color photo-reversible biological switches, often possess two isomeric forms whose spectra overlap. This limits their reversibility when using conventional stationary linear optical excitation [19,20]. But even slightly improving the yield of conversion per pulse of one form with respect to the other may result in dramatic changes in their stationary conversion rates [21]. This can only be done with unconventional nonlinear light sources and we believe double resonance excitation enabled by Raman pre-excitation may be a reasonable choice.

There is much potential for improvement in implementing the technique. In principle, all three pulses could be coherently shaped using pulse-shaping techniques. This would permit optimizing the use of the pump-Stokes spectrum. For example the pump and Stokes pulses could be chirped so that the instantaneous frequency difference would be maintained over a longer time allowing for a higher Raman yield of excitation; in this case, the actinic pulse should be stretched to match the duration of the chirped pump-Stokes pair. Using an automatic laboratory feedback loop [22], a learning algorithm [23–25] could be implemented with the objective function being the relative change of absorption due to the double resonance excitation of one molecule versus another.

With these goals in mind, this work can be seen as the initial step to applying the method of optimal dynamic discrimination (ODD) [26] towards the problem of selective excitation in the presence of spectral crosstalk.

Author Contributions

Y.W. contributed to conceptualization, investigation, visualization, writing - original draft, review and editing, F.L. contributed to data curation, software, validation, writing - original draft, review and editing, A.G. contributed to the development of the original idea of the experiment, selection of the chemical model, investigation, writing - review and editing, H.R. contributed to funding acquisition, resources, writing - review and editing.

Conflicts of interest

"There are no conflicts to declare".

Acknowledgements

The authors acknowledge the financial support of Army Research Office (ARO) No. W911NF-16-1-0014 for experimental aspects of the research and the Department of Energy (DE-FG02-2ER15344) for the theoretical part of the research.

4 Appendix

At the molecular level, the coupling between the electric field and normal vibrational modes is described by the polarizability tensor α_{jk} of the molecule where j, k are molecular Cartesian coordinates. The polarizability can be expressed as a power expansion of the instantaneous normal mode displacement $q(t)$ [15],

$$\alpha_{ij}(t) = \alpha_{ij}^0 + \left(\frac{\partial \alpha}{\partial q}\right)_{ij} q(t) + ... \tag{7}$$

The first order term in $q(t)$ is the origin of Raman scattering. In a two-level system, the expectation value of the displacement $\langle q \rangle$ and the probability δ of finding the molecule with a quanta of vibrational energy in excess of the thermal value $\bar{\delta}$, follow a set of coupled differential equations [15]

$$\left(\frac{\partial^2}{\partial t^2} + \frac{2}{T_2}\frac{\partial}{\partial t} + \omega_0^2\right)\langle q \rangle = \frac{1}{m}F[1 - 2(\delta + \bar{\delta})] \tag{8a}$$

$$\left(\frac{\partial}{\partial t} + \frac{1}{T_1}\right)\delta = \frac{1}{\hbar\omega_0}F\frac{\partial \langle q \rangle}{\partial t}, \tag{8b}$$

where ω_0 is the frequency of the vibrational mode, T_2 and T_1 are, respectively, the coherence time and the lifetime of the excess vibrational population and

$$F = \frac{1}{2}\sum_{i,j}\left(\frac{\partial \alpha}{\partial q}\right)_{ij} E_i E_j$$

is the Raman driving force.

In bulk solution a new set of differential equations governs the growth of the Stokes field $\mathscr{E}_S$ and the buildup of excess vibrational population n as the pump field $\mathscr{E}_P$ propagates through the medium. If the propagation medium and the Raman part of the molecular polarization tensor are isotropic, then the Stokes field and the macroscopic vibrational polarization $\mathscr{Q}$ will be polarized in the same direction as the pump field and $\left(\frac{\partial \alpha}{\partial q}\right)_{ij} = a$ when $i = j$ and 0 when $i \neq j$. To simplify the equations, the E-fields are expressed in their complex forms where

$$\mathscr{E}_P(x,t) = \frac{1}{2}E_P \exp(ik_P x - i\omega_P t)\mathbf{e}_z + c.c.$$

$$\mathscr{E}_S(x,t) = \frac{1}{2}E_S \exp(ik_S x - i\omega_S t)\mathbf{e}_z + c.c.$$

$$\mathscr{Q}(x,t) = \frac{i}{2}Q \exp(ik_0 x - i\omega_0 t)\mathbf{e}_z + c.c.$$

The new equations are [15]

$$\frac{\partial}{\partial x}E_S = \kappa_1 E_P Q^* \tag{9a}$$

$$\left(\frac{\partial}{\partial t'} + \frac{1}{T_2}\right)Q = \kappa_2 E_P E_S^* \tag{9b}$$

$$\left(\frac{\partial}{\partial t'} + \frac{1}{T_1}\right)n = \frac{aN}{8\hbar}\left(E_P E_S^* Q^* + E_P^* E_S Q\right), \tag{9c}$$

where $\kappa_1 = \pi\omega_S^2 aN/c^2 k_S$, $\kappa_2 = a(1 - 2\bar{\delta})/4m(\omega_P - \omega_S)$, $\omega_0 = \omega_P - \omega_S$ and $t' = t - vx$. N denotes the number density of molecules subject to Raman excitation, c the speed of light, v the group velocity of the Stokes field and m is the reduced mass of the vibrational mode. Solutions of Eqs. 9 are [15]

$$E_S(x,t') = E_S(0,t') + E_P(t')\sqrt{bx}\int_{-\infty}^{t'} d\tau \exp\left(\frac{\tau - t'}{T_2}\right) \times \frac{E_P(\tau)E_S(0,\tau)}{\sqrt{W(t') - W(\tau)}} \times I_1\left(2\sqrt{bx[W(t') - W(\tau)]}\right), \tag{10a}$$

$$Q(x,t') = \kappa_2 \int_{-\infty}^{t'} d\tau E_P(\tau)E_S^*(\tau)\exp\left(\frac{\tau - t'}{T_2}\right) \times I_0\left(2\sqrt{bx[W(t') - W(\tau)]}\right), \tag{10b}$$

$$n(x,t') = \frac{aN}{8\hbar}\int_{-\infty}^{t'} [E_P E_S^* Q^* + E_P^* E_S Q]\exp\left(\frac{\tau - t'}{T_1}\right) d\tau \tag{10c}$$

where $b = \kappa_1\kappa_2$, $W(t) = \int_{-\infty}^{t} d\tau |E_P(\tau)|^2$ and I_1, I_0 are Bessel functions of the first kind with complex argument.

When both pump and Stokes E-fields remain unchanged when passing through the sample, the above solutions become independent of x and, consequently, simplify to Eqs. 5 and 6.

For footnotes in the main text of the article please number the footnotes to avoid duplicate symbols. *e.g.* `\footnote[num]{your text}`. The corresponding author $*$ counts as footnote 1, ESI as footnote 2, *e.g.* if there is no ESI, please start at [num]=[2], if ESI is cited in the title please start at [num]=[3] *etc.* Please also cite the ESI within the main body of the text using †.

Notes and references

1 A. Seilmeier, W. Kaiser and A. Laubereau, *Optics Communications*, 1978, **26**, 441–445.

2 A. Seilmeier, W. Kaiser, A. Laubereau and S. Fischer, *Chemical Physics Letters*, 1978, **58**, 225–229.

3 J. C. Wright, *Applied Spectroscopy*, 1980, **34**, 151–157.

4 S. Lee, D. Nguyen and J. Wright, *Applied Spectroscopy*, 1983, **37**, 472–474.

5 C. W. Freudiger, W. Min, B. G. Saar, S. Lu, G. R. Holtom, C. He, J. C. Tsai, J. X. Kang and X. S. Xie, *Science*, 2008, **322**, 1857–1861.

6 C. W. Freudiger, W. Yang, G. R. Holtom, N. Peyghambarian, X. S. Xie and K. Q. Kieu, *Nature Photonics*, 2014, **8**, 153–159.

7 D. Fu, F.-K. Lu, X. Zhang, C. Freudiger, D. R. Pernik, G. Holtom and X. S. Xie, *Journal of the American Chemical Society*, 2012, **134**, 3623–3626.

8 F. Hu, L. Shi and W. Min, *Nature Methods*, 2019, **16**, 830–842.

9 J. W. Lichtman and J.-A. Conchello, *Nature Methods*, 2005, **2**, 910–919.

10 R. Yuste, *Nature Methods*, 2005, **2**, 902–904.

11 Z. Qiang and M. Wang, *ACS Macro Letters*, 2020, **9**, 1342–1356.

12 H. Xiong, L. Shi, L. Wei, Y. Shen, R. Long, Z. Zhao and W. Min, *Nature Photonics*, 2019, **13**, 412–417.

13 H. Xiong and W. Min, *The Journal of Chemical Physics*, 2020, **153**, 210901.

14 K. Iwaszczuk, D. G. Cooke, M. Fujiwara, H. Hashimoto and P. U. Jepsen, *Optics Express*, 2009, **17**, 21969–21976.

15 A. Laubereau and W. Kaiser, *Reviews of Modern Physics*, 1978, **50**, 607.

16 R. N. Jones, *Chemical Reviews*, 1947, **41**, 353–371.

17 N. Gottfried, A. Seilmeier and W. Kaiser, *Chemical Physics Letters*, 1984, **111**, 326–332.

18 H. Shinohara, Y. Yamakita and K. Ohno, *Journal of Molecular Structure*, 1998, **442**, 221–234.

19 V. Emiliani, A. E. Cohen, K. Deisseroth and M. Häusser, *Journal of Neuroscience*, 2015, **35**, 13917–13926.

20 J. J. Tabor, A. Levskaya and C. A. Voigt, *Journal of Molecular Biology*, 2011, **405**, 315–324.

21 Y. Wang, A. Goun, F. Laforge, Z. Quine and H. Rabitz, *Applied Physics Letters*, 2021, **118**, 024101.

22 R. S. Judson and H. Rabitz, *Physical Review Letters*, 1992, **68**, 1500.

23 M. Kumar, M. Husain, N. Upreti and D. Gupta, *Available at SSRN 3529843*, 2010.

24 H.-G. Beyer and H.-P. Schwefel, *Natural Computing*, 2002, **1**, 3–52.

25 M.-L. Zhang and Z.-H. Zhou, *IEEE Transactions on Knowledge and Data Engineering*, 2013, **26**, 1819–1837.

26 M. Roth, L. Guyon, J. Roslund, V. Boutou, F. Courvoisier, J.-P. Wolf and H. Rabitz, *Physical Review Letters*, 2009, **102**, 253001.